ChemComm

RSC Publishing

COMMUNICATION

View Article Online
View Journal

Shape-selected colloidal MOF crystals for aqueous use†

Cite this: DOI: 10.1039/c3cc45935g

Melinda Sindoro,‡[a] Ah-Young Jee‡[b] and Steve Granick*[abc]

Received 3rd August 2013,
Accepted 2nd September 2013

DOI: 10.1039/c3cc45935g

www.rsc.org/chemcomm

Methods are described to synthesize shape-selectable, monodisperse, aqueous-stable metal–organic frameworks (MOFs) by the reaction of aluminium nitrate with benzene tricarboxylic acid in various aqueous solvent mixtures and acetic acid as the capping ligand. Environmental stability was confirmed by thermal analysis and immersion in aqueous acidic media.

The growing appreciation that metal organic frameworks (MOFs) hold interesting potential as colloidal-sized particles, for reasons from scientific[1–4] to applications in areas from separation to sensing,[5–8] presents a new area of opportunity for MOF materials, with potential impact beyond the large relevance that they already enjoy.[9,10] This endeavour requires going beyond the bottom-up design of pore topology and chemical makeup, about which much is already known,[11,12] and to develop methods to control the mesostructure. By this, we mean control over their shape, size, and monodispersity in the colloidal-sized, particulate form. Regulation of MOF geometrical structures is rarely without major change of the pore connectivity, although in selected systems, progress has been made already to regulate the size,[13] uniformity,[14] composition,[15] and morphology[16–20] of colloidal MOFs. Here, looking to potential future applications where particles are immersed in aqueous media, we select a MOF system, an aluminum-based system with benzene tricarboxylic acid linker known as MIL-96,[21] for which the particles are stable in water for extended periods of time. We show a route by which to vary the geometrical morphology of these MOF crystals.

The main idea is that the solvent, in which the synthesis is performed, can act as a modulator. Generally, it is common to regulate crystal shape by introducing modulators (capping agent, surfactants, or polymers) that adsorb preferentially to a favoured crystal facet, consequently inhibiting its relative growth rate.[16–19] But this is not the only possible control variable: from another point of view, the creation of facets can be approached as a crystallization process in which the solvent influences the facet growth rate, growth mode, and stability through its influence on surface supersaturation and temperature.[22] For instance, solvent condition is one of the variables to guide the morphology of biomineral crystals.[23,24] In the MOF field itself, several studies have shown that solvent mixture does play a role in the selecting whether the product will be crystalline or amorphous, single-particle or clusters.[25–27] Fig. 1 summarizes the scheme of this study, and the variety of geometrical structures that have been obtained.

To begin, the colloidal particles were prepared as follows. $Al(NO_3)_3 \cdot 9H_2O$ (0.2 M) and btc, 1,3,5-benzenetricarboxylic acid (0.2 M), were mixed in a 1 : 4 ratio of dimethylformamide (DMF) and water from which pH = 1 was measured. DMF was selected as cosolvent to completely dissolve the btc ligand. To encourage the formation of large and uniform crystals, conditions of slow heating and long incubation time were selected, 130 °C for 24 h, during initial trials. The truncated hexagonal bipyramid (THBP) morphology was obtained (Fig. 2a): two hexagonal facets on the top and the bottom, with twelve trapezoidal facets on the sides,

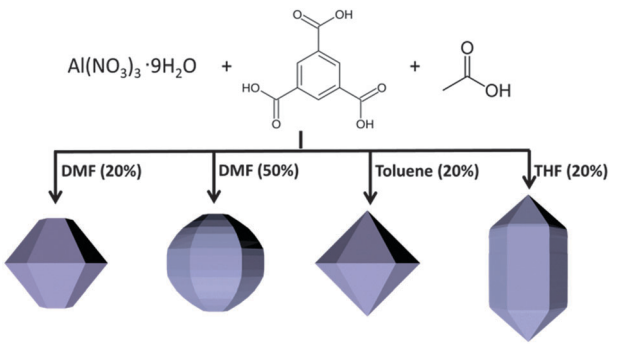

Fig. 1 Scheme of the possible structures obtained in the aqueous synthesis of the aluminum-btc metal organic framework (MOF) known as MIL-96(Al). The basic ingredients are the metal, the organic ligand, and acetic acid; to this, various cosolvents are added as indicated.

[a] Department of Chemistry, University of Illinois, Urbana, Illinois 61801, USA
[b] Department of Materials Science and Engineering, University of Illinois, Urbana, Illinois 61801, USA
[c] Department of Physics, University of Illinois, Urbana, Illinois 61801, USA. E-mail: sgranick@illinois.edu

† Electronic supplementary information (ESI) available. See DOI: 10.1039/c3cc45935g

‡ These authors contributed equally.

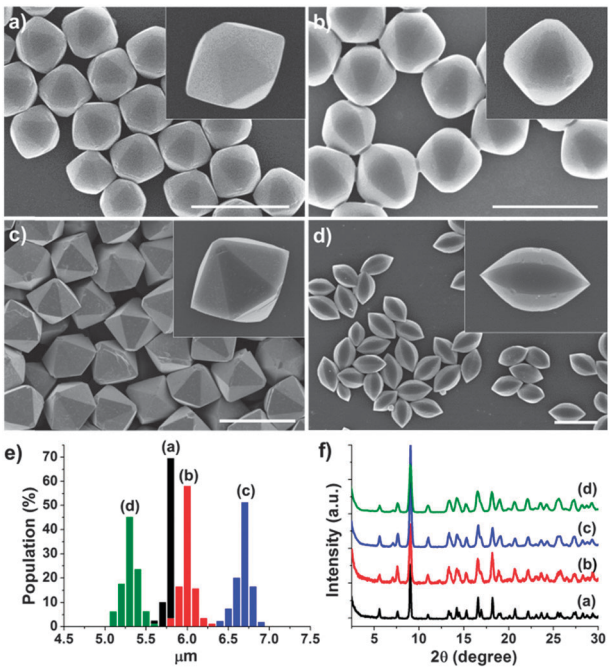

Fig. 2 Scanning electron micrograph (SEM) images and further quantification of them. The SEM images show particles obtained from: (a) 1 : 4 ratio of DMF to water, (b) 1 : 1 ratio of DMF to water, (c) 1 : 4 ratio of toluene to water, and (d) 1 : 4 ratio of THF to water. Scale bars 10 μm. (e) Histogram of the size distribution for each case. (f) Powder X-ray diffraction (XRD) of each case, in which X-ray intensity is plotted against twice the diffraction angle.

each with the average angle of ~120°. These crystals were formed with reasonable polydipersity (12–20 μm, Fig. S1, ESI†) without the need to employ modulator.

To improve monodispersity, the nucleation rate was slowed by adding acetic acid (10 mM), which modulates the deprotonation of btc (pK_a = 3.12, 3.89, 4.70) without altering the relative growth rate of the crystal facets. The particle uniformity was significantly increased (5.8 ± 0.2 μm, Fig. 2e) without any change of geometrical shape. Higher acetic acid concentration decreased the particle size further (Fig. S2a, ESI†) but over only a limited range. When the concentration was doubled (20 mM), the resulting particle were amorphous, and an excess of acetic acid (40 mM) produced only nm-sized particles, as this concentration of acetic acid thoroughly suppresses the deprotonation of btc and stabilizes metal cation complexes,[20,26] preventing the growth of crystal. Accordingly, to regulate the final particle size, we regulated the temperature, finding that the higher the synthesis temperature, the smaller the resulting particles (Fig. S2b, ESI†). This can be reasonably attributed, by known principles of particle synthesis,[28] to a higher nucleation rate such that reactants are distributed between a larger number of growing particles.

Next, the solvent composition was varied while maintaining good solubility for the reactants. Decreasing the water–DMF ratio to 1 : 1 generated a more rounded hexagonal bipyramidal shape (Fig. 2b), close to the original THBP except for smoother transitions between the upper and lower trapezoidal facets. Even lower water–DMF ratios were ineffective, however; they yielded semi-crystalline structures with rough surfaces indicating difficulty to crystallize in the DMF-rich solvent. In separate experiments, toluene (Fig. 2c) and tetrahydrofuran (Fig. 2d) were added as cosolvents. This yielded hexagonal bipyramid (HBP) and spindle-shaped particles respectively. In the case of immiscible cosolvents, heterogenous emulsions may synergistically decrease the nucleation rate.[29] The importance of modulating the nucleation rate is highlighted in the toluene and THF cosolvents without acetic acid. The resulting crystals geometry was very different: it was polydisperse rods and plates (Fig. S4 and S5, ESI†). Furthermore, a control experiment in THF cosolvent showed that modulating the nucleation rate using nitric acid (HNO_3, 10 mM) gave similar spindle shapes (Fig. S6, ESI†). This confirmed that acetic acid did not act as a capping ligand with facet predilection.

To characterize the underlying crystal structures, powder X-ray diffraction (XRD) measurements were made on a Siemens-Bruker D5000 system with CuKα radiation. Fig. 2f shows that the diffraction peaks overlapped, regardless of the method of synthesis. To assess the growth directions, out-of-plane X-ray diffraction measurements were made. As particles of THBP shape lie flat on a surface with one trapezoidal facet parallel to the surface, XRD measurement perpendicular to the surface gives their growth direction. In Fig. 3a, the peak at ~9.12° corresponds to {102} facets. To identify the growth direction at the truncation point, we synthesized a larger THBP particle to obtain larger truncation area and aligned its truncation to the substrate (Fig. 3a). The major peaks at 5.65° and 17.05° correspond to the ⟨002⟩ and ⟨006⟩ directions, allowing us to assign hexagonal truncation as incomplete crystal growth along the *c* axis. We measured similar XRD patterns for the triangular facets of HBP and the trapezoidal facets of rounded THBP particles (Fig. S7, ESI†). As for the spindle shape, which in an SEM micrograph may appear to the eye as quite different, the XRD patterns revealed it to be composed of two elongated hexagonal pyramids seamlessly connected at the long axis. Their alignment parallel to a substrate allowed measurement of the elongated parts. Why spindles formed, rather than rods, could be understood from inspecting the out-of-plane XRD pattern (Fig. 3b), which revealed the existence of {102} facets from the

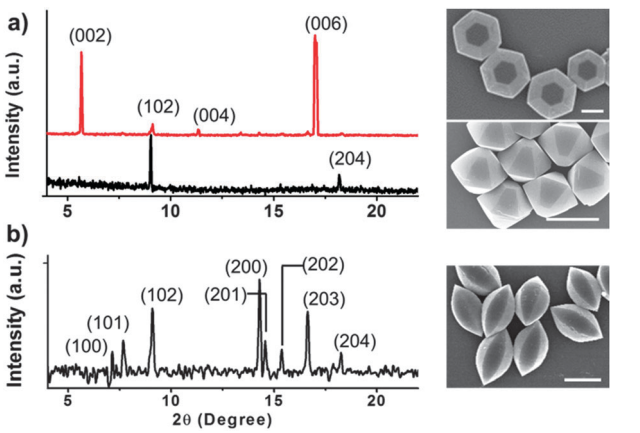

Fig. 3 Out-of-plane XRD patterns of particles aligned on a substrate in various ways: (a) truncated hexagonal bipyramidal (THBP) particles aligned in the truncation direction (top) and aligned along the trapezoid facet (bottom); (b) spindle-shaped particles aligned parallel to their long axis. Scale bars 5 μm.

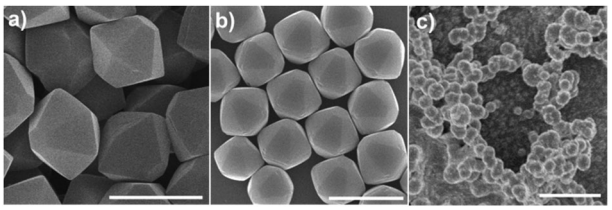

Fig. 4 SEM images of THBP colloidal MIL-96(Al) after (a) 100 days immersion in water (pH = 6) and after 1 day immersion in (b) pH = 1 and (c) pH = 10 respectively. Scale bar 4 μm.

pyramids and growth along the ⟨200⟩ to ⟨204⟩ directions (2θ = 14.29°, 14.65°, 15.46°, 16.68°, 18.38°) as major peaks. Altogether: it seems that DMF slowed growth along the *c* axis, while THF and toluene had the reverse effect, producing elongation. This appears to be how geometrical shape was controlled, without sacrificing size and uniformity of the particles, and without modifying the crystal structure.

In contrast, enhancing the favoured growth rate through pH appeared less effective. When NaOH was added to give initial pH of 4.5, the btc ligand deprotonation was enhanced. The greater availability of btc ligand favoured growth along the *c* axis and yielded hexagonal rods (Fig. S8, ESI†). However, this higher btc concentration was accompanied by fast nucleation, hence producing polydisperse particle size. This typical occurrence was also noted upon amplifying the ratio of ligand by two.

Particle stability was good. First, thermal stability was assessed by thermal gravimetric analysis (TGA) in inert nitrogen environment (Fig. S9, ESI†). The pore volumes (25 wt%) and decomposition temperatures (~550 °C) was comparable to that of bulk MIL-96(Al).[21] To test stability for aqueous use, the particles were immersed in the water for up to 3 months while examining them by scanning electron microscope (SEM) and atomic force microscope (AFM) for possible changes of size and surface roughness, but the average particle size did not change, and the surfaces showed no obvious etching (Fig. S10 and S11, ESI,† respectively). Additional optical measurements of these particles suspended in water suggested that the particles remained stable in extremely acidic condition and up to pH = 8, but not higher (Fig. 4). To achieve environmental stability in a MOF system is challenging because of potential susceptibility to chemicals that oxidize/reduce the metal, or compete with the ligands for coordination to the metal. The encouraging environmental robustness just described suggests the present particles may find uses in aqueous media and environments where the humidity is high.

In summary, colloidal MIL-96(Al) particles can be produced to be monodisperse in size and also in shape, while controlling the geometrical shape by the use of cosolvents as described here. While the crystal shape is not yet predictable without first testing the effect of various cosolvents, the outcome can be rationalized *a posteriori* based on considerations of preferential facet growth. They display excellent stability in neutral-to-acidic aqueous conditions, offering new potential colloidal-based applications for these materials whose pore size is known to be 8.8 Å.

For financial support, we thank grant NSF-CHE-1303757.

Notes and references

1 M. Tsotsalas, A. Umemura, F. Kim, Y. Sakata, J. Reboul, S. Kitagawa and S. Furukawa, *J. Mater. Chem.*, 2012, **22**, 10159–10165.
2 Y. Ikezoe, G. Washino, T. Uemura, S. Kitagawa and H. Matsui, *Nat. Mater.*, 2012, **11**, 1081–1085.
3 H. J. Lee, Y. J. Cho, W. Cho and M. Oh, *Acs Nano*, 2013, **7**, 491–499.
4 N. Yanai, M. Sindoro, J. Yan and S. Granick, *J. Am. Chem. Soc.*, 2013, **135**, 34–37.
5 G. Lu, O. K. Farha, L. E. Kreno, P. M. Schoenecker, K. S. Walton, R. P. Van Duyne and J. T. Hupp, *Adv. Mater.*, 2011, **23**, 4449–4452.
6 E. D. Bloch, W. L. Queen, R. Krishna, J. M. Zadrozny, C. M. Brown and J. R. Long, *Science*, 2012, **335**, 1606–1610.
7 K. M. L. Taylor, W. J. Rieter and W. B. Lin, *J. Am. Chem. Soc.*, 2008, **130**, 14358–14359.
8 W. J. Rieter, K. M. L. Taylor and W. B. Lin, *J. Am. Chem. Soc.*, 2007, **129**, 9852–9853.
9 L. E. Kreno, K. Leong, O. K. Farha, M. Allendorf, R. P. Van Duyne and J. T. Hupp, *Chem. Rev.*, 2012, **112**, 1105–1125.
10 P. Horcajada, R. Gref, T. Baati, P. K. Allan, G. Maurin, P. Couvreur, G. Ferey, R. E. Morris and C. Serre, *Chem. Rev.*, 2012, **112**, 1232–1268.
11 M. O'Keeffe and O. M. Yaghi, *Chem. Rev.*, 2012, **112**, 675–702.
12 T. R. Cook, Y. R. Zheng and P. J. Stang, *Chem. Rev.*, 2013, **113**, 734–777.
13 W. Cho, H. J. Lee and M. Oh, *J. Am. Chem. Soc.*, 2008, **130**, 16943–16946.
14 C. Liu, F. X. Sun, S. Y. Zhou, Y. Y. Tian and G. S. Zhu, *CrystEngComm*, 2012, **14**, 8365–8367.
15 G. Lu, S. Z. Li, Z. Guo, O. K. Farha, B. G. Hauser, X. Y. Qi, Y. Wang, X. Wang, S. Y. Han, X. G. Liu, J. S. DuChene, H. Zhang, Q. C. Zhang, X. D. Chen, J. Ma, S. C. J. Loo, W. D. Wei, Y. H. Yang, J. T. Hupp and F. W. Huo, *Nat. Chem.*, 2012, **4**, 310–316.
16 Q. Liu, L. N. Jin and W. Y. Sun, *Chem. Commun.*, 2012, **48**, 8814–8816.
17 Y. C. Pan, D. Heryadi, F. Zhou, L. Zhao, G. Lestari, H. B. Su and Z. P. Lai, *CrystEngComm*, 2011, **13**, 6937–6940.
18 M. L. Pang, A. J. Cairns, Y. L. Liu, Y. Belmabkhout, H. C. Zeng and M. Eddaoudi, *J. Am. Chem. Soc.*, 2012, **134**, 13176–13179.
19 A. Umemura, S. Diring, S. Furukawa, H. Uehara, T. Tsuruoka and S. Kitagawa, *J. Am. Chem. Soc.*, 2011, **133**, 15506–15513.
20 J. M. Chin, E. Y. Chen, A. G. Menon, H. Y. Tan, A. T. S. Hor, M. K. Schreyer and J. W. Xu, *CrystEngComm*, 2013, **15**, 654–657.
21 T. Loiseau, L. Lecroq, C. Volkringer, J. Marrot, G. Ferey, M. Haouas, F. Taulelle, S. Bourrelly, P. L. Llewellyn and M. Latroche, *J. Am. Chem. Soc.*, 2006, **128**, 10223–10230.
22 C. Giacovazzo, *Fundamentals of Crystallography*, Oxford University Press, New York, 2002.
23 K. M. McGrath, *Adv. Mater.*, 2001, **13**, 989–992.
24 S. Mann, *Angew. Chem., Int. Ed.*, 2000, **39**, 3393–3406.
25 T. Ahnfeldt, N. Guillou, D. Gunzelmann, I. Margiolaki, T. Loiseau, G. Ferey, J. Senker and N. Stock, *Angew. Chem., Int. Ed.*, 2009, **48**, 5163–5166.
26 M. Haouas, C. Volkringer, T. Loiseau, G. Ferey and F. Taulelle, *Chem. Mater.*, 2012, **24**, 2462–2471.
27 P. P. Long, H. W. Wu, Q. Zhao, Y. X. Wang, J. X. Dong and J. P. Li, *Microporous Mesoporous Mater.*, 2011, **142**, 489–493.
28 V. K. Lamer and R. H. Dinegar, *J. Am. Chem. Soc.*, 1950, **72**, 4847–4854.
29 A. Carne, C. Carbonell, I. Imaz and D. Maspoch, *Chem. Soc. Rev.*, 2011, **40**, 291–305.